Atmos. Chem. Phys., 12, 7767–7777, 2012
www.atmos-chem-phys.net/12/7767/2012/
doi:10.5194/acp-12-7767-2012

Atmospheric Chemistry and Physics

Technical Note: Latitude-time variations of atmospheric column-average dry air mole fractions of CO_2, CH_4 and N_2O

R. Saito[1], P. K. Patra[1], N. Deutscher[2,6], D. Wunch[3], K. Ishijima[1], V. Sherlock[4], T. Blumenstock[5], S. Dohe[5], D. Griffith[6], F. Hase[5], P. Heikkinen[7], E. Kyrö[7], R. Macatangay[6], J. Mendonca[8], J. Messerschmidt[3], I. Morino[9], J. Notholt[2], M. Rettinger[10], K. Strong[8], R. Sussmann[10], and T. Warneke[2]

[1]Research Institute for Global Change, JAMSTEC, Yokohama, 236-0001, Japan
[2]Institute of Environmental Physics, University of Bremen, 28359 Bremen, Germany
[3]California Institute of Technology, Pasadena, CA 91125, USA
[4]National Institute of Water and Atmospheric Research (NIWA), Wellington 6021, New Zealand
[5]IMK-ASF, Karlsruhe Institute of Technology (KIT), 76344 Eggenstein-Leopoldshafen, Germany
[6]School of Chemistry, University of Wollongong, NSW, 2522, Australia
[7]FMI-Arctic Research Center, Tähteläntie 62, 99600, Sodankylä, Finland
[8]Department of Physics, University of Toronto, Ontario, M5S 1A7, Canada
[9]National Institute for Environmental Studies (NIES), Tsukuba, 305–8506, Japan
[10]IMK-IFU, Karlsruhe Institute of Technology (KIT), 82467 Garmisch-Partenkirchen, Germany

Correspondence to: R. Saito (rsaito@jamstec.go.jp)

Received: 24 January 2012 – Published in Atmos. Chem. Phys. Discuss.: 22 February 2012
Revised: 17 August 2012 – Accepted: 20 August 2012 – Published: 28 August 2012

Abstract. We present a comparison of an atmospheric general circulation model (AGCM)-based chemistry-transport model (ACTM) simulation with total column measurements of CO_2, CH_4 and N_2O from the Total Carbon Column Observing Network (TCCON). The model is able to capture observed trends, seasonal cycles and inter hemispheric gradients at most sampled locations for all three species. The model-observation agreements are best for CO_2, because the simulation uses fossil fuel inventories and an inverse model estimate of non-fossil fuel fluxes. The ACTM captures much of the observed seasonal variability in CO_2 and N_2O total columns (∼81 % variance, $R > 0.9$ between ACTM and TCCON for 19 out of 22 cases). These results suggest that the transport processes in troposphere and stratosphere are well represented in ACTM. Thus the poor correlation between simulated and observed CH_4 total columns, particularly at tropical and extra-tropical sites, have been attributed to the uncertainties in surface emissions and loss by hydroxyl radicals. While the upward-looking total column measurements of CO_2 contains surface flux signals at various spatial and temporal scales, the N_2O measurements are strongly affected by the concentration variations in the upper troposphere and stratosphere.

1 Introduction

Carbon dioxide (CO_2), methane (CH_4) and nitrous oxide (N_2O) are the major atmospheric greenhouse gases, with a substantial fraction of their emissions coming from anthropogenic activities. Due to the rapid rise in their tropospheric concentrations and significant contribution to anthropogenic radiative forcing during the period of 1750–2005 (Forster et al., 2007 and references therein), these gases are being monitored by in situ (ground-based, airborne) and remote sensing (satellite, ground-based) measurements. Understanding these measurements with the help of chemistry-transport models (CTMs) is critical for interpreting changes in surface fluxes as well as identifying processes that affect flux variations (e.g., Prinn et al., 1990; Keeling et al., 1996; Dlugokencky et al., 2009). Recently, calibrated total column measurements of CO_2, CH_4 and N_2O have become available from the ground-based Total Carbon Column Observing Network (TCCON) (Wunch et al., 2010, 2011). However, recent model-observation comparisons of total columns of CO_2 (defined as X_{CO_2}) have found weaker seasonal cycles for the models at continental sites, which are attributed to model transport errors within the planetary boundary layer or in

the stratosphere or model errors in the seasonal amplitude of surface fluxes (Yang et al., 2007; Keppel-Aleks et al., 2012; Saito et al., 2011, Niwa et al., 2011). Further understanding of the contributions of the tropospheric and stratospheric partial columns to the total columns is required before these new data streams can be used in deriving surface fluxes, in particular for the reactive species (e.g., CH_4, N_2O). The reactive species exhibit a greater decrease rate of concentration with altitude in the stratosphere compared to that of the photochemically inert species, e.g., CO_2.

Parker et al. (2011) compared the TCCON and GOSAT (using the modified retrieval algorithm of the Orbiting Carbon Observatory mission) X_{CH_4} for a whole year within 2009–2010 with a CTM simulation and found that their simulations were lower than TCCON retrievals by ∼30 ppb. Butz et al. (2011) have found that the GOSAT retrievals, by The Netherlands Institute for Space Research (SRON) and Karlsruhe Institute of Technology (KIT), are within ±1.5 ppm (in the range of −0.27 % to +0.49 %) and ±6 ppb (range: −0.53 % to +0.22 %) of the TCCON observations for X_{CO_2} and X_{CH_4}, respectively. Comparison of TCCON and GOSAT retrievals at National Institute of Environmental Studies (NIES) reveal that the GOSAT X_{CO_2} and X_{CH_4} are biased low by 8.85 ppm and 20.4, respectively. These recent inter-comparisons of total columns from remote sensing instruments and models have prompted us to evaluate the simulations of X_{CO_2}, X_{CH_4} and X_{N_2O} by the Center for Climate System Research/National Institute for Environmental Studies/Frontier Research Center for Global Change (CCSR/NIES/FRCGC) AGCM-based CTM (hereinafter, ACTM; Patra et al., 2009; Ishijima et al., 2010; Patra et al., 2011).

Here we compare the simultaneous forward ACTM simulations of X_{CO_2}, X_{CH_4} and X_{N_2O} with TCCON observations, with the main aims of understanding possible causes for the offsets found between model and observations, and the differences between the seasonal cycles among multiple species at a variety of locations. The use of multiple species, with unique properties of their sources, sinks and photochemical loss processes, are shown to be useful for disentangling errors in model total columns due to the surface fluxes and model transport. Such segregation of processes contributing to the total columns measured by remote sensing instruments are required for assimilating this set of observations for source/sink estimations.

2 Model, observation and analysis method

We use the CCSR/NIES/FRCGC AGCM-based chemistry-transport model (i.e., ACTM), which has been developed for simulating the major long-lived greenhouse gases, such as CO_2, CH_4 and N_2O (Patra et al., 2011a, b; Ishijima et al., 2010 and references therein). The ACTM simulations are conducted at T42 spectral truncations in the horizontal (∼2.8× ∼2.8 degrees latitude-longitude) and 67 vertical levels covering the height range from Earth's surface to the mesosphere (∼ 1.3×10^{-5} sigma pressure or ∼80 km). ACTM-simulated vertical profiles of dry mole fractions on the native model grid are sampled for 4 years (2007–2010) at 3-hourly intervals. The simulations were started in 1 January 1980. The representation of transport processes for inter-hemispheric exchange time and inter-latitude gradients of sulfur hexafluoride (SF_6) in ACTM have been validated extensively using in situ measurements (Patra et al., 2011b; Kort et al., 2011 and references therein).

The non-fossil CO_2 fluxes (due to terrestrial biosphere, biomass burning, land-use change and oceanic exchanges) are taken from the 64-region inverse model at monthly-mean time intervals for the year 2008 (Patra et al., 2011a). This set of CO_2 fluxes is repeated for all years. Exclusion of diurnal, synoptic and interannual flux variations in these simulations are likely to introduce some errors in simulating species concentrations. However, as seen from this study, these errors do not affect our analysis of latitudinal and temporal variations significantly. The distribution of emissions due to fossil fuel burning is taken from EDGAR4 (2010) for the year 2005 and global totals are scaled for each year, following Boden et al. (2011). The CH_4 simulations are based on the TransCom control emission scenario extended until the end of 2010, and account for loss due to chemical reactions with hydroxyl radical (OH), chlorine radicals (Cl) and atomic oxygen (O^1D) (Patra et al., 2011b). The tropospheric OH fields are taken from Spivakovsky et al. (2000), and global total is scaled to reproduce CH_3CCl_3 growth rates in the 1990s and 2000s (Patra et al., 2011b). The N_2O fluxes are taken from EDGAR4 and EDGAR2 for land regions, and from Jin and Gruber (2003) for oceanic regions. The soil emissions from EDGAR2 are scaled by factor of 1.2 for producing the observed N_2O growth rates, approximately. Stratospheric loss of N_2O is parameterized using a standard set of photochemical processes (Ishijima et al., 2010).

At each TCCON site, a Fourier Transform Spectrometer (FTS) acquires solar absorption spectra in the near infrared spectral region. Total column amounts are retrieved from these spectra using a least-squares spectral fitting algorithm, GFIT (developed by G. Toon, JPL), which scales a priori mole fraction profiles to provide the best fit to the measured spectra. Total column amounts of CO_2, CH_4 and N_2O, the species of interest here, are ratioed to the retrieved total O_2 column to derive the column-average dry-air mole fractions, X_{CO_2}, X_{CH_4} and X_{N_2O}, respectively. The TCCON is a calibrated network (Deutscher et al., 2010, Wunch et al., 2010; Messerschmidt et al. 2011; Morino et al., 2011), and its error budget, data analysis and other details are described in detail in Wunch et al. (2011). Here, we analyze X_{CO_2}, X_{CH_4} and X_{N_2O} time series at 15 TCCON sites (Table 1 and Fig. 1), namely, Bialystok (BIA), Bremen (BRE), Darwin (DAR), Eureka (EUR),Garmisch (GAR), Izana (IZO), Pasadena (JPL), Karlsruhe (KAR), Lamont (LAM), Lauder

Table 1. List of the TCCON sites used in this study. A comparison between the ACTM and TCCON time series presents the correlation coefficient R, model bias b, model-data difference d, 1-σ standard deviation of residuals (RSD) for observations. We provide three R corresponding to the full time series (TS; Figs. S1–S3 in the Supplement),fitted seasonal cycle (SC; Fig. S5–S7 in the Supplement) and residuals (RS; Figs. S8–S10 in the Supplement) for the observed and model time series.

			X_{CO_2}, ppm						X_{CH_4}, ppb						X_{N_2O}, ppb					
			R			b	d	RSD	R			b	d	RSD	R			b	d	RSD
Site	Latitude	Longitude	TS	SC	RS				TS	SC	RS				TS	SC	RS			
[b]EUR	80.1° N	86.4° W	0.00			1.4	1.7	1.6	0.04			19.8	9.1	6.9	0.79			2.1	1.3	1.9
[b]SOD	67.4° N	26.6° E	0.91			1.0	1.5	3.1	0.57			23.6	16.7	19.8	0.97			5.9	7.4	11.0
BIA	53.2° N	23.0° E	0.88	0.93	0.38	0.9	1.4	3.1	0.51	0.84	0.38	9.4	9.6	12.0	0.88	0.96	0.80	3.7	2.3	4.8
BRE	53.1° N	8.8° E	0.90	0.98	0.25	−0.3	1.4	3.5	0.46	0.91	0.31	2.9	10.5	12.1	0.82	0.95	0.73	1.5	2.8	4.9
[b,a]KAR	49.1° N	8.4° E	0.77			−0.3	1.7	2.6	0.44			−0.9	10.4	12.3						
ORL	48.0° N	2.1° E	0.96	0.90	−0.03	−0.2	1.1	3.6	0.24	0.60	−0.09	0.0	9.3	9.0	0.93	0.98	0.01	1.4	2.1	5.2
GAR	47.5° N	11.1° E	0.85	0.96	0.08	0.3	1.7	3.1	0.36	0.55	0.38	2.7	10.6	10.1	0.86	0.99	0.70	1.4	2.6	4.9
LEF	45.9° N	90.3° W	0.95	0.98	0.02	−0.4	1.2	4.1	0.30	0.28	0.06	4.5	13.2	13.9	0.86	0.94	0.16	0.9	2.5	4.6
LAM	36.6° N	97.5° W	0.88	0.97	0.33	−0.5	1.6	3.0	0.56	0.92	0.32	−15.4	11.9	13.4	0.75	0.95	0.64	−1.6	2.2	3.5
[a]TKB	36.1° N	140.1° E	0.86	0.97	0.31	−0.1	1.5	2.7	0.26	0.20	0.34	−4.5	12.8	10.5						
JPL	34.2° N	118.1° W	0.93	1.00	0.06	−1.4	1.1	2.7	0.60	0.95	0.50	−10.5	10.5	10.9	0.85	0.98	0.77	−1.4	1.8	3.3
[a]IZO	28.3° N	16.5° W	0.96	0.99	0.20	−1.2	0.9	2.4	0.52	0.77	0.45	−13.6	8.0	9.2						
DAR	12.4° S	130.9° E	0.92	0.58	0.30	−0.5	1.0	2.4	0.44	0.03	0.50	−23.6	9.6	10.1	0.69	0.92	0.46	−6.4	1.4	1.9
WOL	34.4° S	150.9° E	0.87	0.72	0.40	0.5	0.8	1.6	0.54	0.65	0.62	−12.1	11.3	12.4	0.84	0.96	0.86	−1.8	1.7	3.0
LAU	45.1° S	169.7° E	0.93	0.63	−0.04	0.0	1.0	2.3	0.72	0.90	0.12	0.0	9.8	13.6	0.77	0.97	0.14	0.0	2.1	3.3

[a] X_{N_2O} are not measured at these sites during the period of this analysis

[b] time series too short for fitting, and thus no calculation of SC and RS components is presented

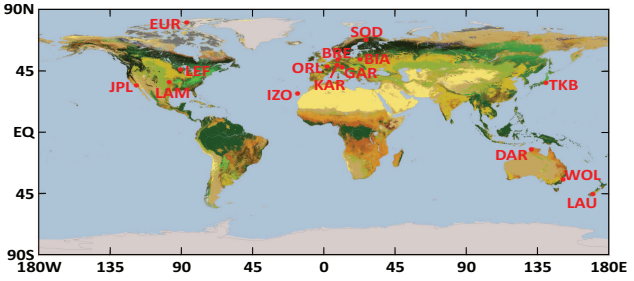

Fig. 1. Locations of TCCON sites (red dots) superimposed on the landcover map (greenish and brownish colors denote intense and weak annual total vegetation activity, respectively; source: www.nasa.gov/vision/earth/environment/urban_effects.html). The full site names and locations can be found in Sect. 2 and Table 1.

(LAU), Orleans (ORL), Park Falls (LEF), Sodankylä (SOD), Tsukuba (TKB) and Wollongong (WOL).

Model equivalents of the TCCON X_y are derived taking the measurement column averaging kernels for the tracer y(CO_2, CH_4 or N_2O) into account. ACTM-simulated profiles of the tracer mole fraction, x_m(P), are extracted for each site. Following Rodgers and Connor (2003), the tracer mole fraction profile x(P) which is integrated to derive the tracer column abundance is given by:

$$x_j = x_{a,j} + A_j(x_{m,j} - x_{a,j}) \quad (1)$$

where $x_{a,j}$ is the TCCON retrieval a priori and A_j is the the TCCON column averaging kernel (a function of solar zenith angle) on the j-th pressure level. The tracer total column abundance is then divided by the corresponding ACTM dry air column abundance to infer the column dry-air mole fraction (DMF; Eqs. A6 and A7 in Wunch et al., 2011). All the ACTM results are adjusted by an offset for X_{CO_2}, X_{CH_4} and X_{N_2O} (ACTM-TCCON = 0 ppm, 25.6 ppb and 3.2 ppb, respectively) to match the average TCCON concentrations at Lauder. Imbalance in surface emissions and loss rates over the time of simulations lead to these offsets in CH_4 and N_2O values. This offset correction is made at the southern-most TCCON site, because the main focus of this study is to understand the seasonal and latitudinal distribution of these species for column distributions.

The partial column (PC) of DMF for the tracer y are calculated as

$$X_{y,\mathrm{tropo}} = \mathrm{PC}_{y,\mathrm{tropo}}/(P_s - P_t) \quad (2)$$

$$X_{y,\mathrm{strato}} = \mathrm{PC}_{y,\mathrm{strato}}/P_t \quad (3)$$

where $\mathrm{PC}_{y,\mathrm{tropo}}$ is the partial column of the tracer from the surface (Ps) to the tropopause (P_t): $\int_{Ps}^{P_t} x(P)dP$ and $\mathrm{PC}_{y,\mathrm{strato}}$ is the partial column of the tracer from the tropopause (P_t) to the top of the atmosphere (x_{H_2O}(P) assumed = 0 for simplicity) and the corresponding dry air partial columns are given by $\int_{P_{\max}}^{P_{\min}} dP$.

For quantitative evaluation of the model-observation agreement, we prepared following statistics: correlation coefficient R, model bias b [=$\Sigma(X^{ACTM}-X^{TCCON})/N$]; where N is the number of data points in the time series, and standard deviations of model-data difference d [=sqrt{$\Sigma(X^{ACTM}-X^{TCCON})^2/N$}]. We use the digital filtering method described in Nakazawa et al. (1997) for decomposing the daily averaged original time series (model and observations separately) into long-term trend (periodicity

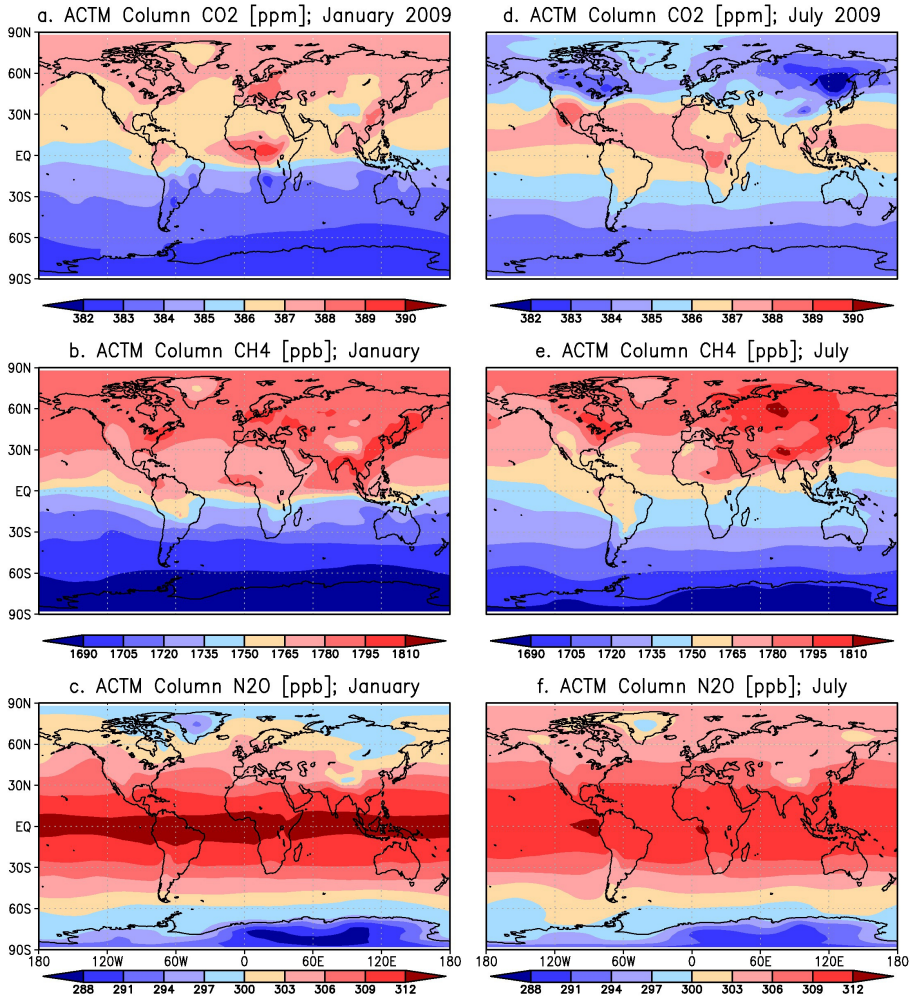

Fig. 2. Monthly mean global distributions of the ACTM-simulated total column CO_2, CH_4 and N_2O (without applying averaging kernel and a priori smoothing) in January (left column) and July (right column) 2009.

longer than 24 months) and fitted curve (without the high-frequency variations). The seasonal cycles for each species at different sites are calculated by subtracting the long-term trends from the fitted time series, and the residuals (representing synoptic variability) are calculated by subtracting the fitted time series from the original time series.

3 Results and discussions

3.1 Global distributions

The latitude-longitude distributions of ACTM-simulated CO_2, CH_4 and N_2O column-average dry-air mole fractions (DMFs) are shown in Fig. 2. Global DMFs presented in Fig. 2 are calculated by taking TCCON averaging kernels, A to be the unit vector. The ACTM-simulated X_{CO_2} distribution shows values about 5 ppm higher in the northern hemisphere (NH) than the southern hemisphere (SH) in January. During July, the average X_{CO_2} values in mid-high latitudes (pole-wards of 45°) of both hemispheres show similar concentrations, with values in the tropics higher by about 4 ppm. The inter-hemispheric (IH) gradients (defined as NH minus SH) of X_{CH_4} are about 100 ppb both in January and July, indicating CH_4 sources in the NH dominate sinks by the reaction with OH in all seasons. This is contrary to the CH_4 distribution near the Earth's surface, where the CH_4 IH gradient is as strong as 250 ppb in January and much weaker (∼150 ppb) in July (Patra et al., 2009). Despite higher CH_4 emissions in July, lower CH_4 concentrations near the surface are caused by the stronger vertical transport and loss of CH_4 due to its reaction with OH. Since the vertically transported CH_4 resides in the middle and upper troposphere, the differences in X_{CH_4} with seasons are not distinct, compared to the surface concentrations. The X_{N_2O} are always higher in the tropics by at least 5 ppb compared to the high latitudes (∼60°) in both the hemispheres, and particularly low values are seen over the Antarctic region and Greenland reflecting

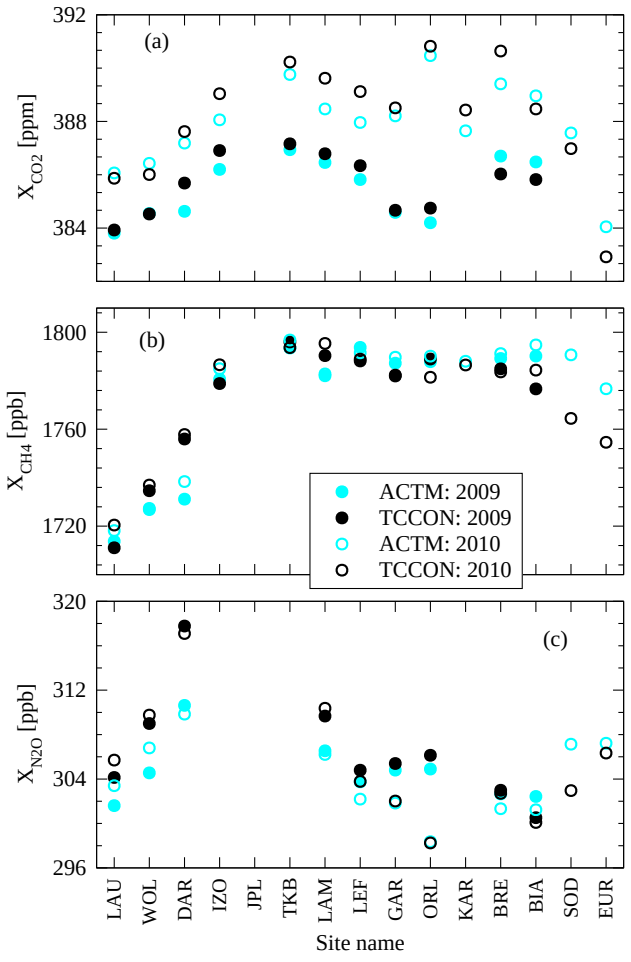

Fig. 3. Observed (black) and simulated (blue) values of X_{CO_2} (top), X_{CH_4} (middle) and X_{N_2O} (bottom) at the TCCON sites. Annual mean values for 2009 and 2010 are shown for this comparison (note that there are data gaps in time series for both years). The sites are arranged by latitude from Lauder to Eureka, located at the highest latitudes in the SH and NH, respectively.

the meridional gradient in tropopause height. During January the tropical upwelling branch of the Brewer-Dobson circulation is narrow and N_2O-rich air is transported deep in to the stratosphere (240 ppb isopleths reach beyond 10 mb), while during July similar N_2O concentrations reside below 10 mb but over wider tropical latitudes (Ishijima et al., 2010). Thus the peak in N_2O column over the equator is more flattened in July than in January.

Figure 3 compares the annual mean X_y observed and simulated by ACTM at TCCON sites. The model is able to simulate annual mean X_{CO_2}, X_{CH_4} and X_{N_2O} at the sites (ordered by latitudes along the x-axis) within about 1 ppm, 10 ppb and 2 ppb, respectively, at most sites. In these comparisons the model is sampled at the observation times, thus larger differences between the average values for 2010 and 2009 at GAR and ORL are mainly caused by differences in the months of data coverage, while other sites are showing an average CO_2 growth rate of ∼2 ppm between 2009 and 2010. The TCCON X_{CO_2} are higher by about 2 ppm than ACTM X_{CO_2} in 2010 at both LAM and LEF, while agreement between TCCON and ACTM were good in 2009. This mismatch in 2010 is produced by shallower seasonal cycle minimum for X_{CO_2} at the two sites (Fig. 4). The summer drought in temperate North America may have led to weaker terrestrial ecosystem uptake in 2010. Such differences in annual average values for N_2O are also seen, but are less distinct for CH_4, which has relatively weaker seasonal amplitudes (and hence less influence from the timing of the data gap). The latitudinal variations of X_{CO_2} and X_{CH_4} are in general agreement with those observed within the troposphere. However, the X_{N_2O}variations are in contrast with the N_2O IH gradients at the surface or in the upper troposphere of about 1 ppb (Prinn et al., 1990; Ishijima et al., 2010). The X_{N_2O} variations are related to variations in tropopause height, indicating stronger stratospheric influence on the X_{N_2O} abundance, compared to the surface fluxes (further details in Sect. 3.4).

3.2 Model and observed time series

Comparisons between the ACTM (blue dots) and TCCON (black dots) time series of X_{CO_2}, X_{CH_4} and X_{N_2O} for 2007–2010 are shown for seven selected sites at hourly time intervals in Fig. 4. The ACTM-simulated values with no smoothing by averaging kernels are shown as a 3-hourly continuous time series (thin brown line). The model time series, created from the data points sampled at TCCON observation times and after applying the averaging kernels and a priori profiles, is shown by blue dots. The X_{CO_2} comparisons between the ACTM and TCCON time series show that the model bias b at each site is within ±1.0 ppm, except at Eureka (1. 4 ppm), JPL (−1.4 ppm) and Izana (−1.2 ppm) (refer to Fig. 5 and Table 1 for detailed statistics).

The time series are highly correlated ($R > 0.8$), suggesting a realistic representation of transport and fluxes in ACTM for simulating X_{CO_2} seasonal cycle and trends. This is despite the fact that interannual variability in non-fossil fluxes is not accounted for in ACTM, and that the fossil fuel emission map is based on the EDGAR4 distribution for a single year (2005). The model-data differences d are slightly smaller in the SH (∼1 ppm) than those at the NH continental sites (<1.8 ppm).

The goodness of model-observation agreement may also be defined with respect to the residual data variability at a particular site. The 1-σ standard deviation of residuals (RSDs) for the measured time series are given in Table 1. If model-data differences (b and d) are less than the observed RSDs, the model-observation agreement can be considered good. We find, both b and d are generally smaller or similar in magnitude compared to the observed RSD at all sites for X_{CO_2}, X_{CH_4} and X_{N_2O}.

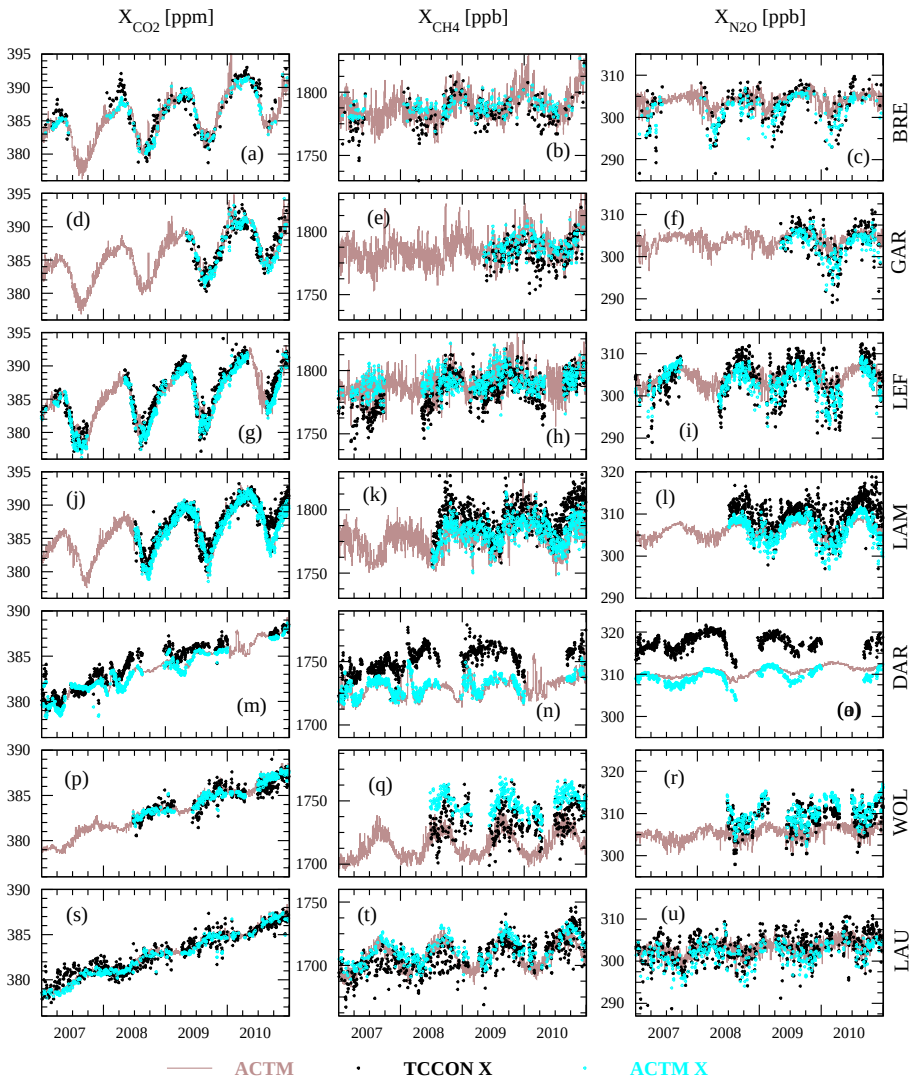

Fig. 4. Comparisons of TCCON measurement (black dots) and ACTM-simulation smoothed by averaging kernels and a priori profiles (blue dots) for X_{CO_2}, X_{CH_4}, and X_{N_2O} (from left to right panels) at seven selected sites (corresponding names marked on the right for each row). The observational records at the other operational TCCON sites are short or do not cover all three species. The brown line represents the original/unsmoothed ACTM continuous time series with a 3-hourly time step. Comparisons of X_{CO_2}, X_{CH_4} and X_{N_2O} from TCCON and ACTM are depicted for all measurement sites in Fig. S1, S2 and S3, respectively.

The time series of the ACTM X_{CH_4} (blue dots) compared with the subset of TCCON X_{CH_4} (black dots) is shown in the middle column panels in Fig. 4. The correlation coefficients between observed and simulated time series are generally greater than 0.3, except at Orleans and Tsukuba (Fig. 5 and Table 1). The model biases *b* are relatively large at Eureka (19.8 ppb) and Sodankyla (23.6 ppb), Lamont (−15.4 ppb), JPL (−10.5 ppb), Izana (−13.6 ppb), Darwin (−23.6 ppb) and Wollongong (−12.1 ppb), and less than ∼10 ppb at the other sites. Model-data comparisons of X_{CO_2} and surface CH_4 concentrations (Patra et al., 2009, 2011b) would suggest ACTM inter hemispheric transport is not the source of relatively large biases in X_{CH_4}. Rather, we speculate these are driven by errors in regionally varying emissions, tropospheric chemistry, and transport across the tropopause. The model-data differences *d* are less than 13 ppb (except at Sodankyla), which are more uniform across the sites than the more widely varying biases.

The right panels in Fig. 4 show X_{N_2O} time series of the ACTM (blue dots) and TCCON (black dots). The impact of applying averaging kernels and a priori profiles to ACTM X_{N_2O} is clearly seen in two ways: (1) the absolute values are adjusted higher and agree better with the TCCON measurements at the tropical and sub-tropical sites, and (2) the amplitude of daily and seasonal variability increases significantly (blue dots) from those without applying the averaging

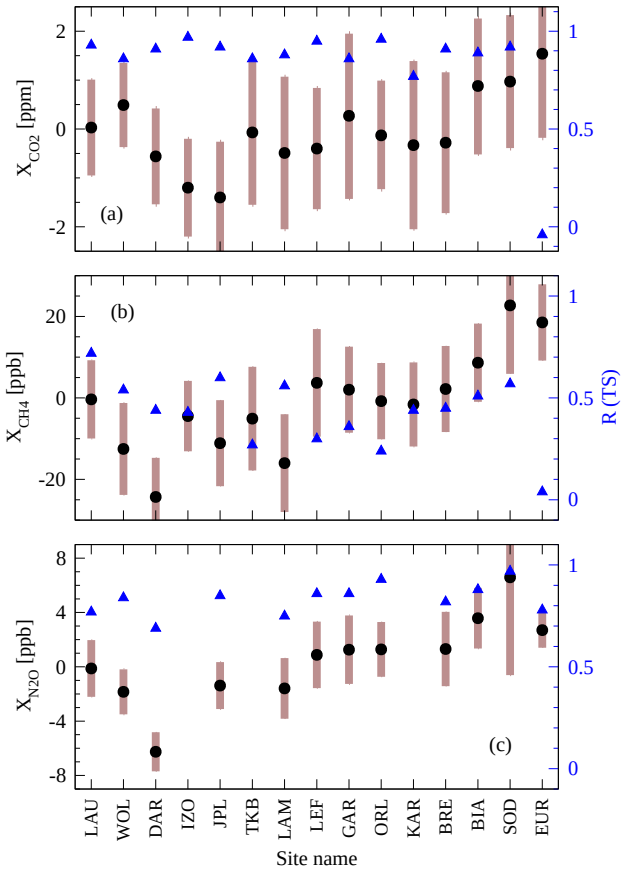

Fig. 5. The model bias b (black dots) and model-data difference d (brown bars) for **(a)** X_{CO_2}, **(b)** X_{CH_4}, and **(c)** X_{N_2O}. Correlation coefficient R (blue symbols) corresponds to the y-axis on right. No observations are available for X_{N_2O} at Izana, Tsukuba,and Karlsruhe. Biases corresponding to four seasons are shown in Fig. S4.

kernel (thin brown line). This is because the TCCON X_{N_2O} averaging kernels have higher sensitivity in the stratosphere (Fig. 4 of Wunch et al., 2011), effectively amplifying variations in the total column abundance of N_2O due to variations in tropopause height, and hence leading to more variability in X_{N_2O} than that observed in N_2O mixing ratios near the Earth's surface (Ishijima et al., 2010). For example, the TCCON averaging kernels for N_2O increase from 0.5 in the lower troposphere to more than 1.5 at 100 mb at a solar zenith angle of 20° over Lamont, while those for CO_2 and CH_4 increase only by 50 % in the same altitude range. Thus the TCCON FTS spectra are more sensitive to the troposphere and surface fluxes for CO_2 and CH_4 compared to N_2O. The correlation coefficient of the time series is high ($R > 0.7$) at every site. The model biases b at Wollongong, Darwin, JPL, and Lamont are negative (−1.4, −6.4, −1.8, and −1.6, respectively), similar to the latitudinal variations for X_{CH_4}. The model-data differences d at all sites are <3 ppb, except at Sodankyla (Fig. 5).

Larger bias and differences at Sodankyla for X_{CH_4} and X_{N_2O} are due to ACTM-TCCON differences in spring (Fig. S4 in the Supplement), which is a dynamically active period at this latitude, related to the movement of the Arctic polar vortex. The ACTM simulations show higher N_2O concentration within the polar spring vortex compared to the measurements from limb-viewing satellites (Ishijima et al., 2010). The systematically high values for measured X_{CH_4} and X_{N_2O} compared to the simulation for sites between Wollongong and Lamont (34.4° S to 36.6° N) may arise from higher tropical tropopause heights due to coarse horizontal resolution of the model failing to reproduce the sharp gradient in tropopause height between the equator and 30° latitude (e.g., Patra et al., 2011b). It is also known that the N_2O sources in the tropical regions as used in this simulation are underestimated (Kort et al., 2011), particularly in Southeast Asia, which can affect the N_2O concentrations around Darwin significantly. However, the ACTM-simulated IH gradients for all three species are in close agreement with the TCCON measurements, e.g., the ACTM-TCCON differences in annual mean X_{CO_2}, X_{CH_4} and X_{N_2O} at all sites are generally within 1.5 ppm, 20 ppb and 2 ppb, respectively, and with no apparent seasonal bias (except at Sodankyla and Darwin).

3.3 Comparison of seasonal cycles and residuals

The seasonal cycles from the measured and simulated time series are obtained by removing long-term trends both from the fitted smooth curve and raw data as described in Sect. 2. Peak-to-trough amplitudes and the phase of the cycles in ACTM X_{CO_2} are in very good agreement with those of TCCON X_{CO_2} at the NH sites (Fig. S5 in the Suppelement; R for SC in Table 1). For example, no apparent mismatches can be found at the Tsukuba, JPL, Park Falls and Bremen sites for the 2007–2010 period. These results show better agreement than previous studies (Basu et al., 2011; Keppel-Aleks et al., 2012). This improvement is potentially associated with differences in the surface fluxes and transport model. At Orléans and Bialystok, about a month delay in the ACTM X_{CO_2} seasonal cycle phase is observed compared with that measured by TCCON. Noteworthy here is that the inverse model fluxes have only monthly time resolution and only four large regions over western Europe. European sites Bremen, Bialystok and Orleans all fall in the same model region, and hence the model simulates the same phase of seasonality (in agreement with Bremen), while the TCCON measurements at those sites differ. An inversion at finer spatial and temporal resolution may help distinguish the flux heterogeneity between sites.

Among the sites consisting of more than one year of data coverage, we find the seasonal cycle amplitudes are overestimated by about 2 ppm at Izana and Lamont, unlike previous studies, which report an underestimation of X_{CO_2} peak-to-trough amplitudes (e.g., Yang et al., 2007; Basu et al., 2011). In particular, when the seasonal cycle amplitude and phase

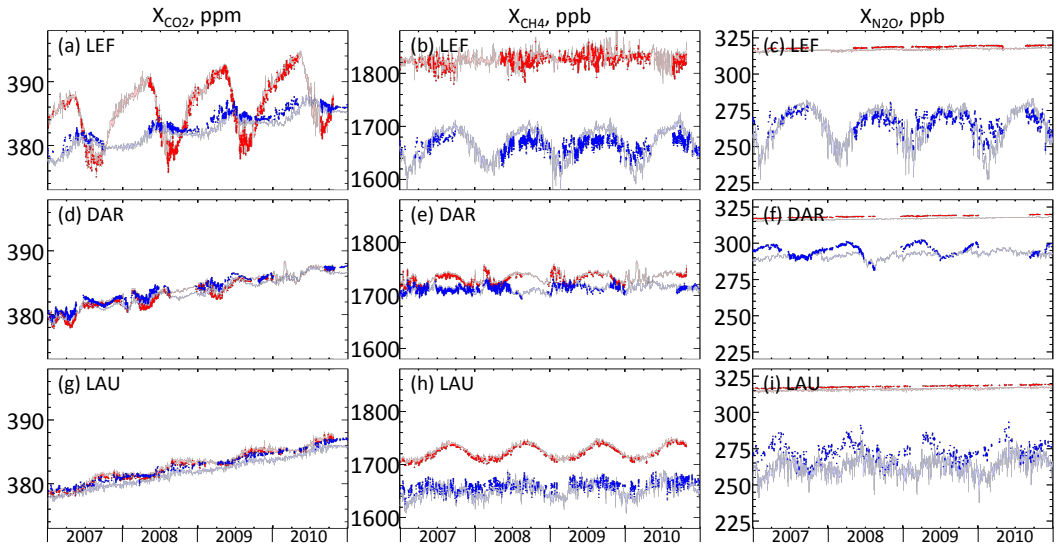

Fig. 6. Time series of ACTM partial columns in the troposphere (in red) and stratosphere (in blue) for CO_2 (left column), CH_4 (middle column) and N_2O (right column) at threes elected sites representing northern and southern midlatitudes and tropics. Continuous lines in lighter colours show the partial columns before smoothing by averaging kernels and a priori profiles. The tropospheric and stratospheric partial columns for monthly varying and annual mean tropopause are shown in Figs. S11 and S12.

are in good agreement at Park Falls, the anomalously deep seasonal uptake at Lamont arises from bias in the inverse model flux. This is because the estimated summer uptake is influenced by the nearest northern site (Park Falls), which has stronger uptake due to denser vegetation and agricultural activities compared to the regions around the Lamont site (Fig. 1). The four regions of temperate North America in the 64-region inverse model do not provide sufficient degrees of freedom for capturing these ecological differences between sites. Note also that the continental CO_2 measurement sites within the 4 temperate North America regions of Patra et al. (2011a) inversions are located north of 40° N Thus, the X_{CO_2} distributions at TCCON measurement sites contain significant new information on the local-regional surface fluxes.

The extraction of X_{CH_4} seasonal cycle information from the TCCON measurements is affected by the signal-to-noise ratio and data gaps (Fig. S6). At the SH sites, the daily and synoptic variabilities (residuals) are as large as the seasonal cycle, which affects the Darwin site most, followed by Wollongong and Lauder. It is also likely that some of the local and regional sources of CH_4 are not included in the ACTM simulations (e.g., Fraser et al., 2011). However, the relatively high correlation coefficients for residuals at Darwin and Wollongong indicate realistic representation of CH_4 emission distribution and synoptic transport in ACTM over Australia. At Park Falls and Lamont, dense data coverage leads to better seasonal cycle extraction, and we find that the ACTM and TCCON X_{CH_4} time series are highly correlated. Generally, the correlation coefficient of the X_{CH_4} time series between the ACTM and TCCON is lower than 0.7 at all sites, which is significantly less than for X_{CO_2} or X_{N_2O} (Table 1).

The X_{N_2O} seasonal cycles are in excellent agreement ($R >$ 0.92) at most sites except for NH high latitudes (Fig. S7; Table 1), suggesting the seasonal variations of N_2O loss rates in the stratosphere and the seasonal variation of tropopause height are fairly well represented in the ACTM. The residual variability, presumably due to synoptic variation in tropopause height and stratosphere-troposphere exchange events, is reasonably well represented at some (Bialystok, Bremen, Garmisch, Pasadena, Wollongong), but not all TCCON sites.

3.4 Characteristics of partial columns in the troposphere and stratosphere

Figure 6 shows the time series of modeled dry-mole fraction partial columns of CO_2, CH_4 and N_2O using Eqs. (2 and 3) for the period of 2007–2010. These comparisons suggest that most of the variability in the total columns of CO_2 and CH_4 is from the tropospheric column (Figs. 4 and 6). While the N_2O seasonal cycle amplitudes near the Earth's surface are typically within 1 ppb, the total column abundances vary by more than 10 ppb with seasons. The larger fraction of the X_{N_2O} seasonal cycle amplitude is contributed by the stratospheric part of the column. The high correlation coefficients for ACTM and TCCON X_{N_2O} at all time scales and sites suggest that the ACTM is capable of simulating the variations in stratospheric photochemical loss (mostly seasonally varying) and daily-synoptic scale variability in transport in the upper troposphere and lower stratosphere (UT/LS) region. Note here that the N_2O averaging kernels are more sensitive to the UT/LS height region than in the troposphere, and that the

derived X_{N_2O} are sensitive to the stratosphere-troposphere exchange (STE) processes.

4 Conclusions

The ACTM-simulated dry-air column-averaged mole fractions of CO_2, CH_4 and N_2O are compared with observed time series at 15 TCCON sites. TCCON measurement averaging kernels and retrieval a priori are taken into account to derive model equivalents of the TCCON observations. Weighting by the TCCON column averaging kernels has the largest impact on X_{N_2O} and its variability, compared with that for X_{CH_4} and X_{CO_2}. The model fairly successfully captures the seasonal cycle amplitude and phase as well as the inter-latitude gradients between most sites for all three species. The correlation coefficients for ACTM and TCCON X_{CO_2} and X_{N_2O} are mostly over 0.9 for seasonal cycles. The model-observation differences (*b* and *d*) are mostly found to be below the observed residual variability in the observed time series. Our results suggest the measured X_{CO_2} is sensitive to the surface flux heterogeneity between continental sites in Europe and North America and should have implications for inverse estimations of regional sources/sinks.

However, the model-observation comparisons of X_{N_2O} do not provide conclusive evidence of a surface emission signal in total column observations, which largely contain the signal of N_2O variability due to tropopause altitude variability. The underestimation of ACTM X_{CH_4} in comparison with TCCON observations clearly indicate a need for greater emissions at the Earth's surface or reduction in tropospheric loss between the Wollongong (34° S) and Lamont (37° N) sites. The role of model transport uncertainty as the cause of this X_{CH_4} underestimation is ruled out because ACTM can simulate fairly well the observed X_{N_2O} variations associated with the UT/LS and altitudes above. Thus the stratospheric contribution to the tracer column DMFs must be accounted for accurately if total column data are to provide useful constraints on the surface fluxes of trace gases with stratospheric photochemical sinks. Some test cases are available for separating the tropospheric partial column of CH_4 using hydrogen fluoride (HF) stratospheric columns (Washenfelder et al., 2003). Similarly, another conservated quantity, the 'age' of stratospheric air, may also be used for estimating stratospheric partial columns (e.g., Saito et al., 2011).

Supplementary material related to this article is available online at: http://www.atmos-chem-phys.net/12/7767/2012/acp-12-7767-2012-supplement.pdf.

Acknowledgements. The ACTM model results will be made available freely to the scientific and policymaking communities upon request. This work is partly supported by JSPS/MEXT KAKENHI-A (grant number22241008), and Asia Pacific Network (APN). We thank Paul Wennberg for useful discussions. US funding for TCCON comes from NASA's Terrestrial Ecology Program, grant number NNX11AG01G, the Orbiting Carbon Observatory Program, the Atmospheric CO_2 Observations from Space (ACOS) Program and the DOE/ARM Program. The Darwin TCCON site was built at Caltech with funding from the OCO project, and is operated by the University of Wollongong, with travel funds for maintenance and equipment costs funded by the OCO-2 project. We acknowledge funding to support Darwin and Wollongong from the Australian Research Council, Projects LE0668470, DP0879468, DP110103118 and LP0562346. Lauder TCCON measurements are funded by New Zealand Foundation of Research Science and Technology contracts C01X0204 and CO1X0406. We acknowledge financial support of the Bialystok and Orléans TCCON sites from the Senate of Bremen and EU projects IMECC, GEOMON and InGOS as well as maintenance and logistical work provided by AeroMeteo Service (Bialystok) and the RAMCES team at LSCE (Gif-sur-Yvette,France) and additional operational funding from the NIES GOSAT project. The Garmisch TCCON team acknowledges funding by the EC-INGOS project. Measurements at Eureka were made by the Canadian Network for Detection of Atmospheric Composition Change (CANDAC) with additional support from the Canadian Space Agency. Complete acknowledgment text for all sites can be found on the TCCON website (https://tccon-wiki.caltech.edu/).

Edited by: I. Aben

References

Basu, S., Houweling, S., Peters, W., Sweeney, C., Machida, T., Maksyutov, S., Patra, P. K., Chevallier, F., Niwa, Y., Matsueda, H., and Sawa, Y.: The seasonal cycle amplitude of total column CO_2: Factors behind the model-observation mismatch, J. Geophys. Res., 116, D23306, doi:10.1029/2011JD016124, 2011.

Boden, T. A., Marland, G., and Andres, R. J.: Global, Regional, and National Fossil-Fuel CO_2 Emissions. Carbon Dioxide Information Analysis Center, Oak Ridge National Laboratory, US Department of Energy, Oak Ridge, Tenn., USA, 2011.

Butz, A., Guerlet, S., Hasekamp, O., Schepers, D., Galli, A., Aben, I., Frankenberg, C., Hartmann, J. -M., Tran, H., Kuze, A., Keppel Aleks, G., Toon, G., Wunch, D., Wennberg, P., Deutscher, N., Griffith, D., Macatangay, R., Messerschmidt, J., Notholt, J., and Warneke, T.: Toward accurate CO_2 and CH_4 observations from GOSAT, Geophys. Res. Lett., 38, L14812, doi:10.1029/2011GL047888, 2011.

Deutscher, N. M., Griffith, D. W. T., Bryant, G. W., Wennberg, P. O., Toon, G. C., Washenfelder, R. A., Keppel-Aleks, G., Wunch, D., Yavin, Y., Allen, N. T., Blavier, J. -F., Jiménez, R., Daube, B. C., Bright, A. V., Matross, D. M., Wofsy, S. C., and Park, S.: Total column CO_2 measurements at Darwin, Australia – site description and calibration against in situ aircraft profiles, Atmos. Meas. Tech., 3, 947–958, doi:10.5194/amt-3-947-2010, 2010.

Dlugokencky, E. J., Bruhwiler, L., White, J. W. C., Emmons, L. K., Novelli, P. C., Montzka, S. A., Masarie, K. A., Lang, P. M., Crotwell, A. M., Miller, J. B., and Gatti, L. V. : Observational constraints on recent increases in the atmospheric CH_4 burden,

Geophys. Res. Lett., 36, L18803, doi:10.1029/2009GL039780, 2009.

EDGAR4: European Commission, Joint Research Centre (JRC)/Netherlands Environmental Assessment Agency (PBL), Emission Database for Global Atmospheric Research (EDGAR), release version 4. x., http://edgar.jrc.ec.europa.eu, 2010.

Forster, P., Ramaswamy, V., Artaxo, P., Berntsen, T., Betts, R., Fahey, D., Haywood, J., Lean, J., Lowe, D., Myhre, G., Nganga, J., Prinn, R. G., Raga, M. S., and Dorland, R. V.: Changes in Atmospheric Constituents and in Radiative Forcing, Climate Change 2007: The Physical Science Basis, Contribution of Working Group I to the Fourth Assessment Report of the Intergovernmental Panel on Climate Change – IPCC, 2007.

Fraser, A., Chan Miller, C., Palmer, P. I., Deutscher, N. M., Jones, N. B., and Griffith, D. W. T.: The Australian methane budget: Interpreting surface and train-borne measurements using a chemistry transport model, J. Geophys. Res., 116, D20306, doi:10.1029/2011JD015964, 2011.

Ishijima, K., Patra, P. K., Takigawa, M., Machida, T., Matsueda, H., Sawa, Y., Steele, L. P., Krummel, P. B., Langenfelds, R. L., Aoki, S., and Nakazawa, T.: Stratospheric influence on the seasonal cycle of nitrous oxide in the troposphere as deduced from aircraft observations and model simulations, J. Geophys. Res., 115, D20308, doi:10.1029/2009JD013322, 2010.

Jin, X. and Gruber, N.: Offsetting the radiative benefit of ocean iron fertilization by enhancing N_2O emissions, Geophys. Res. Lett., 30, 2249, doi:10.1029/2003GL018458, 2003.

Keeling, C. D., Chin, J. F. S., and Whorf, T. P.: Increased activity of northern vegetation inferred from atmospheric CO_2 measurements, Nature, 382, 146–149, 1996.

Keppel-Aleks, G., Wennberg, P. O., Washenfelder, R. A., Wunch, D., Schneider, T., Toon, G. C., Andres, R. J., Blavier, J.-F., Connor, B., Davis, K. J., Desai, A. R., Messerschmidt, J., Notholt, J., Roehl, C. M., Sherlock, V., Stephens, B. B., Vay, S. A., and Wofsy, S. C.: The imprint of surface fluxes and transport on variations in total column carbon dioxide, Biogeosciences, 9, 875–891, doi:10.5194/bg-9-875-2012, 2012.

Kort, E. A., Patra, P. K., Ishijima, K., Daube, B. C. , Jiménez, R., Elkins, J., Hurst, D., Moore, F. L., Sweeney, C., and Wofsy, S. C.: Tropospheric distribution and variability of N_2O: evidence for strong tropical emissions, Geophys. Res. Lett., 38, L15806, doi:10.1029/2011GL047612, 2011.

Messerschmidt, J., Geibel, M. C., Blumenstock, T., Chen, H., Deutscher, N. M., Engel, A., Feist, D. G., Gerbig, C., Gisi, M., Hase, F., Katrynski, K., Kolle, O., Lavrič, J. V., Notholt, J., Palm, M., Ramonet, M., Rettinger, M., Schmidt, M., Sussmann, R., Toon, G. C., Truong, F., Warneke, T., Wennberg, P. O., Wunch, D., and Xueref-Remy, I.: Calibration of TCCON column-averaged CO_2: the first aircraft campaign over European TCCON sites, Atmos. Chem. Phys., 11, 10765–10777, doi:10.5194/acp-11-10765-2011, 2011.

Morino, I., Uchino, O., Inoue, M., Yoshida, Y., Yokota, T., Wennberg, P. O., Toon, G. C., Wunch, D., Roehl, C. M., Notholt, J., Warneke, T., Messerschmidt, J., Griffith, D. W. T., Deutscher, N. M., Sherlock, V., Connor, B., Robinson, J., Sussmann, R., and Rettinger, M. : Preliminary validation of column-averaged volume mixing ratios of carbon dioxide and methane retrieved from GOSAT short-wavelength infrared spectra, Atmos. Meas. Tech., 4, 1061–1076, doi:10.5194/amt-4-1061-2011, 2011.

Nakazawa, T., Ishizawa, M., Higuchi, K., and Trivett, N. B. A.: Two curve fitting methods applied to CO_2 flask data, Environmetrics, 8, 197–218, 1997.

Niwa, Y., Patra, P. K., Sawa, Y., Machida, T., Matsueda, H., Belikov, D., Maki, T., Ikegami, M., Imasu, R., Maksyutov, S., Oda, T., Satoh, M., and Takigawa, M.: Three-dimensional variations of atmospheric CO_2: aircraft measurements and multi-transport model simulations, Atmos. Chem. Phys., 11, 13359–13375, doi:10.5194/acp-11-13359-2011, 2011.

Parker, R., Boesch, H., Cogan, A., Fraser, A., Feng, L., Palmer, P. I., Messerschmidt, J., Deutscher, N., Griffith, D. W. T., Notholt, J. ,Wennberg, P. O., and Wunch, D. : Methane observations from the Greenhouse Gases Observing SATellite: Comparison to ground-based TCCON data and model calculations, Geophys. Res. Lett., 38, L15807, doi:10.1029/2011GL047871, 2011.

Patra, P. K., Takigawa, M., Ishijima, K., Choi, B. -C., Cunnold, D., Dlugokencky, E. J., Fraser, P., Gomez-Pelaez, A. J., Goo, T. -Y., Kim, J. -S., Krummel, P., Langenfelds, R., Meinhardt, F., Mukai, H., O'Doherty, S., Prinn, R. G., Simmonds, P., Steele, P., Tohjima, Y., Tsuboi, K., Uhse, K., Weiss, R., Worthy, D., and Nakazawa, T. : Growth rate, seasonal, synoptic, diurnal variations and budget of methane in lower atmosphere, J. Meteorol. Soc. Jpn., 87, 635–663, 2009.

Patra, P. K., Niwa, Y., Schuck, T. J., Brenninkmeijer, C. A. M., Machida, T., Matsueda, H., and Sawa, Y.: Carbon balance of South Asia constrained by passenger aircraft CO_2 measurements, Atmos. Chem. Phys., 11, 4163–4175, doi:10.5194/acp-11-4163-2011, 2011.

Patra, P. K., Houweling, S., Krol, M., Bousquet, P., Belikov, D., Bergmann, D., Bian, H., Cameron-Smith, P., Chipperfield, M. P., Corbin, K., Fortems-Cheiney, A., Fraser, A., Gloor, E., Hess, P., Ito, A., Kawa, S. R., Law, R. M., Loh, Z., Maksyutov, S., Meng, L., Palmer, P. I., Prinn, R. G., Rigby, M., Saito, R., and Wilson, C.: TransCom model simulations of CH4 and related species: linking transport, surface flux and chemical loss with CH_4 variability in the troposphere and lower stratosphere, Atmos. Chem. Phys., 11, 12813–12837, doi:10.5194/acp-11-12813-2011, 2011.

Prinn, R., Cunnold, D., Rasmussen, R., Simmonds, P., Alyea, F., Crawford, A., Fraser, P., and Rosen, R.: Atmospheric emissions and trends of nitrous oxide deduced from 10 years of ALE GAGE data, J. Geophys. Res., 95, 18369–18385, doi:10.1029/JD095iD11p18369, 1990.

Rodgers, C. and Connor, B.: Intercomparison of remote sounding instruments, J. Geophys. Res, 108, 4116–4229, 2003.

Saito, R., Houweling, S., Patra, P. K., Belikov, D., Lokupitiya, R., Niwa, Y., Chevallier, F., Saeki, T., and Maksyutov, S.: TransCom satellite intercomparison experiment: Construction of a bias corrected atmospheric CO_2 climatology, J. Geophys. Res., 116, D21120, doi:10.1029/2011JD016033, 2011.

Washenfelder, R. A., Wennberg, P. O., and Toon, G. C.: Tropospheric methane retrieved from ground-based near-IR solar absorption spectra, Geophys. Res. Lett., 30, 2226, doi:10.1029/2003GL017969, 2003.

Wunch, D., Toon, G. C., Wennberg, P. O., Wofsy, S. C., Stephens, B. B., Fischer, M. L., Uchino, O., Abshire, J. B., Bernath, P., Biraud, S. C., Blavier, J. -F. L., Boone, C., Bowman, K. P., Browell, E. V., Campos, T., Connor, B. J., Daube, B. C., Deutscher, N. M., Diao, M., Elkins, J. W., Gerbig, C., Gottlieb, E., Griffith, D. W. T., Hurst, D. F., Jiménez, R., Keppel-Aleks, G., Kort, E. A.,

Macatangay, R., Machida, T., Matsueda, H., Moore, F., Morino, I., Park, S., Robinson, J., Roehl, C. M., Sawa, Y., Sherlock, V., Sweeney, C., Tanaka, T., and Zondlo, M. A. : Calibration of the Total Carbon Column Observing Network using aircraft profile data, Atmos. Meas. Tech., 3, 1351–1362, doi:10.5194/amt-3-1351-2010, 2010.

Wunch, D., Toon, G. C., Blavier, J.-F. L., Washenfelder, R. A., Notholt, J., Connor, B. J., Griffith, D. W. T., Sherlock, V., and Wennberg, P. O.: The Total Carbon Column Observing Network, Philos. T. Roy. Soc. A, 369, 2087–2112, doi:10.1098/rsta.2010.0240, 2011.

Yang, Z., Washenfelder, R., Keppel-Aleks, G., Krakauer, N., Randerson, J., Tans, P., Sweeney, C., and Wennberg, P.: New constraints on Northern Hemisphere growing season net flux, Geophys. Res. Lett., 34, L12807, doi:10.1029/2007GL029742, 2007.